Environmental Science and Ecotechnology 29 (2026) 100659

Contents lists available at ScienceDirect

Environmental Science and Ecotechnology

journal homepage: www.journals.elsevier.com/environmental-science-and-ecotechnology/

Original Research

OVOCs drive radical cycling and ozone formation in background air

Enyu Xiong [a,b,c], Hai Guo [c,*], Tzung-May Fu [a,b,**], Xiaopu Lyu [d], Yu Wang [c], Beining Zhou [c], Men Xia [c,e,f,d], Zhouxing Zou [c], Qi Yuan [c], Jin Yang [c], Kit Ying Shek [c], Jiongkai Chen [a,b], Tianci Jiang [a,b], Wei Tao [a,b], Aoxing Zhang [a,b], Wang Xiang [a,b], Shuncheng Lee [c,g], Tao Wang [c]

[a] State Key Laboratory of Soil Pollution Control and Safety, Shenzhen Key Laboratory of Precision Measurement and Early Warning Technology for Urban Environmental Health Risks, School of Environmental Science and Engineering, Southern University of Science and Technology, Shenzhen, Guangdong, 518055, China
[b] Guangdong Provincial Field Observation and Research Station for Coastal Atmosphere and Climate of the Greater Bay Area, Southern University of Science and Technology, Shenzhen, Guangdong, 518055, China
[c] Department of Civil and Environmental Engineering, The Hong Kong Polytechnic University, Hong Kong SAR, 999077, China
[d] Department of Geography, Hong Kong Baptist University, Hong Kong SAR, 999077, China
[e] Aerosol and Haze Laboratory, Beijing Advanced Innovation Center for Soft Matter Science and Engineering, Beijing University of Chemical Technology, Beijing, 100029, China
[f] Institute for Atmospheric and Earth System Research, Faculty of Science, University of Helsinki, Helsinki, 00014, Finland
[g] Function Hub of Sustainable Energy and Environment, The Hong Kong University of Science and Technology (Guangzhou), Guangzhou, Guangdong, 511455, China

ARTICLE INFO

Article history:
Received 8 May 2025
Received in revised form
11 January 2026
Accepted 12 January 2026

Keywords:
Surface ozone
Radical budget
Oxygenated volatile organic compounds
Photochemistry
Methylglyoxal
Biacetyl
Pearl river delta

ABSTRACT

Surface ozone pollution is a critical global environmental challenge driven by the complex, nonlinear photochemical cycling of RO_x radicals (OH + HO_2 + RO_2). Oxygenated volatile organic compounds (OVOCs) are central to these cycles as both radical sources and sinks, yet their quantitative impact on regional radical budgets remains poorly understood due to historical limitations in ambient measurements. This knowledge gap hinders the accurate prediction of persistent ozone exceedances. Here we show that constraining atmospheric models with a broad suite of 23 OVOCs—specifically reactive dicarbonyls—is essential for the accurate simulation of radical chemistry in southern China's background air through comprehensive field observations and photochemical modeling. We find that models constrained with only the three most common OVOCs (formaldehyde, acetaldehyde, and acetone) overestimate hydroxyl radical concentrations by 50%–100%, whereas comprehensive constraints align simulations with observations. This discrepancy is caused by complex offsetting errors, including the severe overestimation of isoprene-derived intermediates and the significant underestimation of secondary biacetyl production. Our results reveal that photolysis of the measured OVOCs contributes 49–61% of total RO_x production, with species such as methylglyoxal and biacetyl playing unexpectedly dominant roles in driving ozone formation. These findings highlight critical deficiencies in current chemical mechanisms and demonstrate that high-resolution monitoring of reactive OVOC intermediates is vital for developing effective emission control strategies to mitigate persistent regional ozone pollution.

* Corresponding author.
** Corresponding author. State Key Laboratory of Soil Pollution Control and Safety, Shenzhen Key Laboratory of Precision Measurement and Early Warning Technology for Urban Environmental Health Risks, School of Environmental Science and Engineering, Southern University of Science and Technology, Shenzhen, Guangdong, 518055, China.
E-mail addresses: hai.guo@polyu.edu.hk (H. Guo), fuzm@sustech.edu.cn (T.-M. Fu).

https://doi.org/10.1016/j.ese.2026.100659

1. Introduction

Surface ozone (O_3) pollution is a critical environmental challenge in China despite aggressive controls of precursor emissions, such as NO_x (defined as NO + NO_2) and volatile organic compounds (VOCs) [1,2]. In the Pearl River Delta region (PRD) of Southern China, O_3 has been the principal pollutant in exceedances of the national air quality standards since 2015 [3]. O_3 forms photochemically via nonlinear, NO_x-catalyzed cycling of RO_x radicals—a family of highly reactive species consisting of hydroxyl (OH), hydroperoxyl (HO_2), and organic peroxyl (RO_2) [4]. Quantifying RO_x budgets is therefore critical for understanding the cause of the persistent surface O_3 pollution. In particular, oxygenated volatile organic compounds (OVOCs) are key intermediates in VOC oxidation and act as both sources and sinks of RO_x [5,6]. However, the quantitative impact of OVOCs on RO_x remains uncertain, partly because ambient OVOC measurements have historically been sparse. Early studies either did not measure OVOCs or measured only a limited subset (e.g., formaldehyde, acetaldehyde, and acetone) [7] at low temporal resolution due to a lack of cost-effective online sampling and analytical methods as well as commercial gas standards for many OVOCs [8,9].

Advancements in *in situ* measurement and remote sensing technologies now enable observations of a broader suite of OVOCs at high temporal resolutions [10–12], elucidating their significant role in shaping ambient OH levels, RO_x cycling, and O_3 production [13,14]. Recent studies in the PRD have shown that accounting for the OH reactivity of additional OVOC variants reduces the "missing OH source" identified in early studies [15,16]. Studies have also underscored that photolysis of OVOCs is a major source of RO_x [17–19], challenging past theories that RO_x predominantly originates from O_3 photolysis in rural areas [20,21] and from nitrous acid (HONO) photolysis in urban areas [22–24]. Research has further highlighted that dicarbonyls exert disproportionate impacts on RO_x and O_3. For example, at an urban site in Guangdong in autumn, photolysis of methylglyoxal contributed more than 25% of the RO_x generated from non-formaldehyde OVOCs [19]. Research in Hong Kong showed that the three dicarbonyls (glyoxal, biacetyl, and methylglyoxal) accounted for only 2% of ambient OVOC concentrations but 13% of the total O_3 formation potential associated with OVOCs [25]. These findings highlight the critical role of OVOCs in RO_x budgeting and O_3 formation. However, the specific pathways and impacts of individual OVOCs require further investigation.

In this study, we conducted and analyzed direct measurements of O_3, OH, 63 VOCs, 23 OVOCs, and other precursors at a regional background PRD site in October to November 2020. Our comprehensive measurements enabled us to analyze the impacts of these OVOCs on the local RO_x budget and O_3 photochemistry in unprecedented detail. We explored how constraining a photochemical box model with observations of different suites of OVOC species affects simulated OH abundance and the RO_x budget. We then traced the discrepancies to the key OVOCs and precursors that caused them and analyzed O_3 formation. These analyses elucidate how OVOCs drive photochemistry and O_3 formation in background PRD air and highlight key gaps in the field's knowledge of photochemical mechanisms.

2. Materials and methods

2.1. Field measurements at Hok Tsui and categorization of three photochemical cases

We conducted a field measurement campaign at the Hok Tsui Supersite (HT; 22.3° N, 114.3° E; Supplementary Fig. S1), located at the southeastern edge of the PRD region, from October 7 to November 6, 2020 (Supplementary Text S1). Briefly, we measured continuous ambient concentrations of O_3, OH, nitrous acid (HONO), NO_x, CO, SO_2, and C_1–C_8 OVOCs; the photolysis frequency of NO_2 ($j(NO_2)$); and relevant meteorological variables (Supplementary Table S1) [13,26]. OH concentrations were measured using a nitrate-quadrupole chemical ionization mass spectrometer (THS Inc., Atlanta, Georgia, United States) [13]. C_1–C_8 OVOCs were measured online using a proton transfer reaction time-of-flight mass spectrometry system (PTR-QiToF-MS, IONICON Analytik, Innsbruck, Austria) [27].

During the ten-day campaign (October 7, 8, 10, 11, and 20–22, and November 3, 4, and 6, 2020), we collected ambient whole-air samples in 2 L canisters at 2 h intervals from 09:00 to 18:00 local time (LT). The VOCs were analyzed offline using a gas chromatography-mass spectrometer system equipped with mass-selective detection, electron capture detection, and flame ionization detection (GC-MS/MSD/ECD/FID, Agilent 5973N, Santa Clara, California, United States) (Supplementary Text S1). In total, 63 VOC species and 23 OVOC species were included in the subsequent analyses. Notably, we also measured the ambient concentrations of two dicarbonyls: methylglyoxal and biacetyl (2,3-butanedione).

We categorized the photochemical conditions on each of the ten days of VOC sampling according to the 72-h back-trajectories calculated using the hybrid single-particle Lagrangian integrated trajectory model (HYSPLIT) (Supplementary Fig. S1 and Text S1d) [28]. Air masses sampled on October 7, 8, and 20–22 and on November 3 were transported from the inner PRD to HT and thus categorized as continental. On November 6, the surface maximum daily 8-h average O_3 concentration in Hong Kong (97 ppb, 190 μg m^{-3}) exceeded the Chinese National Ambient Air Quality Standard of 160 μg m^{-3}. This O_3 pollution event was associated with synoptic subsidence and stagnant surface conditions induced by an approaching tropical storm (Atsani; Supplementary Fig. S2), which was the dominant meteorological pattern driving O_3 pollution in the PRD in fall [21,29]. Accordingly, that day was categorized as an O_3 pollution case. Measurements on October 10 and 11 and November 4 were categorized under the coastal case because the sampled air masses had been transported along the coastline of Eastern China.

2.2. Setup of the F0AM box model and sensitivity simulations

We used the Framework for 0-D Atmospheric Modeling (F0AM v.4.2) box model [30], which incorporates the Master Chemical Mechanism (MCM v3.3.1; http://mcm.york.ac.uk/, last accessed: July 1, 2024) [31–33] to simulate photochemistry at HT. Each simulation was spun up for 72 h to achieve a steady state. We assumed a 24-h lifetime for all free-running chemical species against first-order local physical loss processes (i.e., ventilation and deposition), consistent with the diurnal boundary layer dynamics at this subtropical coastal site and the observed strong diurnal variability in all VOCs and OVOCs during the measurement period. Further details, including assumed HONO production rates on a day marked by instrument failure (November 6), bias corrections for simulated photolysis rates and for formaldehyde measurements altered by humidity, and sensitivity tests examining the irreversible heterogeneous uptake of methylglyoxal and glyoxal on aqueous aerosol surfaces [34,35], are described in Supplementary Text S2, Fig. S3, and Fig. S4.

For each of the three photochemical cases, we performed two sensitivity experiments (Table 1): a baseline configuration (BASE) and a more extensive OVOC-constrained configuration (CON23). BASE experiments were constrained with observed concentrations of trace gases, HONO, 63 VOCs, and the three most commonly

Table 1
Design of F0AM sensitivity experiments using different observational constraints.

Experiments	Observational constraints
BASE	Meteorological parameters, $j(NO_2)$, trace gases (NO, NO_2, SO_2, CO, O_3), HONO, 63 VOCs, and 3 OVOCs (formaldehyde, acetaldehyde, acetone)
CON23	Meteorological parameters, $j(NO_2)$, trace gases (NO, NO_2, SO_2, CO, O_3), HONO, 63 VOCs, 3 OVOCs (formaldehyde, acetaldehyde, acetone), and an additional 20 OVOCs (including methylglyoxal, biacetyl, MVK + MACR).

measured OVOC species (formaldehyde, acetaldehyde, and acetone), following the methods previously reported in most photochemical budget studies [7,18,22]. All 63 VOCs were observationally constrained using canister measurements to ensure data consistency. In CON23 experiments, we further constrained F0AM with the observed concentrations of all 23 OVOC species, including the two measured dicarbonyls. All other configurations were the same for the BASE and CON23 experiments.

3. Results and discussion

3.1. High OVOC and aromatic concentrations observed in HT

The meteorological and photochemical conditions observed at HT during the measurement periods were typical of the PRD region for October and November (Fig. 1, Supplementary Tables S2 and S3). Throughout the sampling period, the weather at HT was warm, sunny, and humid, with a prevailing northeasterly. The mean daytime (09:00–18:00 LT) O_3 concentration was 31% lower in the continental case (47 ± 16 ppb) than in the coastal case (68 ± 13 ppb). The coastal case involved 16% stronger solar radiation ($j(NO_2) = 5.0 \times 10^{-3}\ s^{-1}$) and 13% lower average wind speeds (4.5 ms^{-1}) than the continental case. Additionally, the NO_x level was approximately 50% lower in the coastal case (2.0 ppb vs. 3.9 ppb in the continental case), which weakened the titration of O_3 by NO. These meteorological and chemical factors enhanced local photochemical production while reducing dispersion, promoting a more favorable environment for O_3 accumulation in the coastal case. On the day O_3 exceedance was observed (November 6, when the mean daytime O_3 was 79 ppb), most of Southern China was impacted by the subsiding outflow of the approaching Tropical Storm ATSANI (Supplementary Fig. S2), creating hot, sunny, and stagnant conditions at the surface.

By integrating VOC measurements from the canister GC-MS/MSD/FID/ECD analyses with OVOC measurements from PTR-ToF-MS, we comprehensively characterized the VOC/OVOC composition of the regional background air. The composition of total VOCs (TVOCs) was relatively stable throughout the sampling period (Supplementary Fig. S1c and Table S3), with the largest contributions coming from OVOCs (65–72%), followed by alkanes (16–22%), aromatics (6–8%), alkenes (6–7%), and alkyl nitrates (<0.1%). This result underscores the prominence of OVOCs in the background air at HT. High percentages of OVOCs in TVOCs have been reported in previous studies conducted in the PRD using comparable

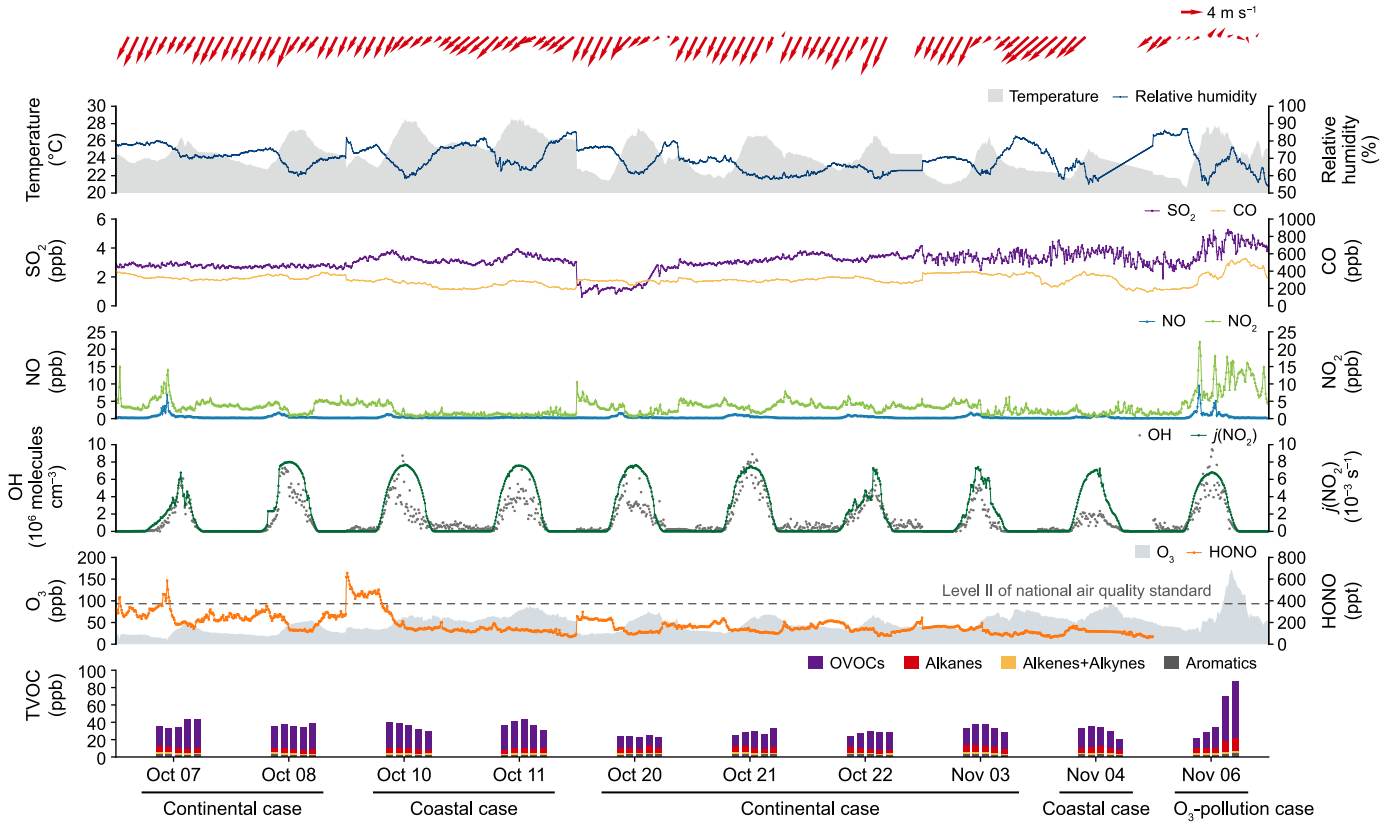

Fig. 1. Observed trace gases concentrations of sulfur dioxide (SO_2), carbon monoxide (CO), NO (nitric oxide), NO_2 (nitrogen dioxide), OH (hydroxyl radical), O_3 (ozone), HONO (nitrous acid) and TVOCs (total VOCs) and meteorological conditions at Hok Tsui Supersite on the ten volatile organic compound sampling days in fall 2020. Red arrows indicated wind speed and wind direction and $j(NO_2)$ indicated photolysis frequency of NO_2.

measurement techniques. For instance, Wu et al. [9] reported a high percentage of OVOCs in TVOCs (57 ± 10%) in urban Guangzhou in autumn 2018—a value slightly lower than ours due to more abundant precursor VOCs in urban air. Other studies conducted in fall 2020 that used only PTR-ToF-MS reported OVOC fractions of up to 90% in urban Guangzhou [36] and 77% at a coastal site in Hong Kong [36]. These higher OVOC percentages may be biased high due to the limited ability of PTR-ToF-MS to detect alkanes. That potential bias notwithstanding, our measurements corroborate past findings in highlighting the predominance of OVOCs in the ambient PRD air in fall.

Throughout the campaign, concentrations of reactive VOCs and OVOCs were recorded at moderate to high levels compared to values previously reported in the PRD. Isoprene (0.48 ppb) was the most abundant alkene across all cases, as it was during earlier campaigns at HT [20,37]. The daytime (06:00–18:00 LT) mean concentration of C_8 aromatics (m/p-xylene, o-xylene, and ethylbenzene) was 0.9 ppb, which was slightly lower than the values previously reported at suburban sites in the PRD [36,38] but 2.9 and 3.4 times the levels observed at HT in fall 2012 [20] and fall 2018 [37], respectively (Supplementary Table S4). C_9 aromatic concentrations (trimethylbenzenes, 0.3 ppb) were 18–57% higher than those in urban Shantou [38] and Guangzhou [9,39] yet 2.5 times lower than those in urban Shenzhen (0.7 ppb) [40]. This pattern suggests that the HT site was influenced by industrial and solvent-related emissions originating from the upwind PRD region [41]. Among the measured OVOCs, methanol accounted for the largest fraction (25%), followed by acetone, acetic acid, acetaldehyde, and formaldehyde. In contrast, ethanol and acetaldehyde were the most abundant OVOC species in the air of urban Guangzhou (24%) [42] and suburban Hong Kong (54%) [36], respectively, highlighting differences in precursors and photochemistry across urban, suburban, and coastal air in the PRD. The two measured dicarbonyls (0.2 ± 0.1 ppb methylglyoxal and 0.3 ± 0.3 ppb biacetyl) constituted only 2% of the daytime total measured OVOC concentrations, consistent with the measurements of Xu et al. [25].

3.2. Observational constraints on more OVOCs improved simulated OH concentrations

OH radical concentration is commonly used to evaluate *in situ* box modeling performance [43]. Fig. 2 and S5 (Supplementary Material) compare observed and simulated OH concentrations when the F0AM model was constrained with different OVOC measurements. Table S4 (Supplementary Material) summarizes the simulated concentrations of OH, HO_2, and RO_2 for each of the three photochemical cases in the BASE and CON23 experiments. In the BASE experiments, the ratios of simulated versus observed ($R_{S/O}$) daytime (06:00–18:00 LT) mean OH concentrations were 1.5 and 2.0 for the continental and coastal cases, respectively, indicating that the model overestimated OH beyond the 44% measurement uncertainty [9]. These overestimations were similar to those found in previous studies, in which the photochemical models were constrained with observations of a small number of OVOCs [13,44,45].

In comparison, when F0AM was constrained with measurements of all 23 OVOCs (the CON23 experiments, Table 1), the simulated OH concentrations aligned more closely with the observations in the continental ($R_{S/O}$ = 1.1) and coastal ($R_{S/O}$ = 1.3) cases in terms of diurnal variation and magnitude (Fig. 2a and b). In the O_3 pollution case, the BASE ($R_{S/O}$ = 1.6) and CON23 ($R_{S/O}$ = 1.3) experiments both simulated OH concentrations within the variable observed ranges; nevertheless, the CON23 simulations were closer to the observed mean (Fig. 2c). This consistency between observed and CON23-simulated OH for all three photochemical cases is markedly improved compared to earlier studies in the PRD, whose models neglected either substantial sources [24] or substantial sinks [13] of OH. We found that the lower OH levels simulated in the CON23 experiments resulted from a 7% lower OH production rate (Supplementary Fig. S6) and a 6% higher OH reactivity (Supplementary Fig. S7) relative to the BASE experiments. The reduced OH production in the CON23 experiments was driven mainly by a weaker HO_2 + NO reaction, which was attributable in turn to less HO_2 production when more OVOC species were observationally constrained (Supplementary Fig. S6). The effects of observational constraints on OH reactivity were more nuanced. CON23 simulated lower OH reactivity associated with methylglyoxal (from 13% to 2%), and the sum of methyl vinyl ketone (MVK) and methacrolein (MACR) (from 18% to 4%). In contrast, OH reactivity from other OVOCs increased, most notably for methanol (from 1% to 6%), the sum of methyl ethyl ketone (MEK) and butanal (from 0.3% to 4%), and for carboxylic acids (from 0.2% to 9%) (Supplementary Fig. S7c and S7d). These distinct contributions of individual OVOCs highlight the critical impact of comprehensive OVOC constraints on local photochemical budgets.

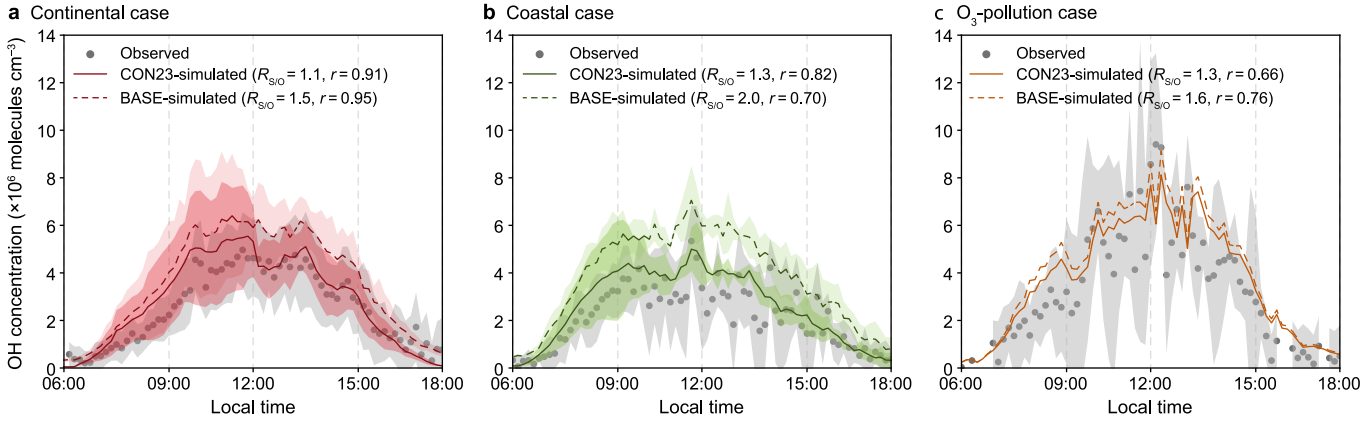

Fig. 2. Diurnal variation in OH at Hok Tsui Supersite across three photochemical cases. Observed and simulated OH concentrations are shown for the continental (**a**), coastal (**b**), and O_3-pollution (**c**) cases. The shaded areas indicate standard deviations of the observed and simulated concentrations. Insets report the ratio of simulated to observed daytime (06:00–18:00 local time) mean OH concentrations ($R_{S/O}$) and the daytime temporal correlations (r).

3.3. OVOC photolysis as the dominant RO_x source at HT and mechanistic biases in the BASE experiment

For all three photochemical cases, the simulated OH concentrations in the CON23 experiments were more consistent with the observed OH concentrations compared to those simulated in the BASE experiments. This improved agreement of the CON23 experiments, given OH's central role in RO_x cycling, supports a realistic RO_x budget at HT. We analyzed the model's results to identify the key species and pathways that affect the RO_x budget at HT. Fig. 3 shows that photolysis of OVOCs was the dominant source (49–61%) of RO_x in the ambient air at HT across all cases, regardless of whether 3 or 23 OVOC constraints were applied. This finding contrasts with a previous study at HT in fall 2012, which identified the dominant source of RO_x as O_3 photolysis (47%), followed by OVOC photolysis (33%) [20]. Li et al. [20] constrained only five OVOC species (formaldehyde, acetaldehyde, acetone, propanal, and benzaldehyde) and only at low temporal resolution (24-h averages), potentially suppressing their model's ability to accurately resolve fast photochemical processes. Similarly, our finding that OVOC photolysis was the dominant RO_x source contrasts with other studies (18–41%) that used fewer OVOC species as constraints, including studies at other sites in the PRD [21,24,46] and other major cities in China [47,48] and the United States [44,49] during photochemical seasons. Our findings corroborate those of Wang et al. [19], who constrained more than 20 OVOCs in urban Guangzhou and found that OVOC photolysis contributed 43%–59% of total RO_x production in fall. The greater contribution of OVOC photolysis to RO_x production in our study reflects the substantial role of OVOCs in radical production, a role that has been underrepresented in previous studies with limited measurement capabilities.

The simulated loss pathways of RO_x were similar regardless of whether 3 or 23 OVOCs were constrained, but they differed between non-O_3 pollution and pollution periods (Fig. 3). In the continental and coastal cases, RO_x was mainly lost to the $HO_2 + RO_2$ (31–49%) and $HO_2 + HO_2$ (15–21%) reactions. In contrast, during the O_3 pollution case, RO_x was most quickly removed via $OH + NO_x$ (NO and NO_2) (38%) and $RO_2 + NO_2$ reactions (48%, forming peroxyacetyl nitrate). These findings contradict earlier measurements at HT in 2012, when $OH + NO_x$ dominated the RO_x sink pathways [20]. This difference likely reflects the reduction in NO_x emissions in the PRD area in recent years and underscores the importance of OVOCs in driving current O_3 pollution [50].

We next considered which OVOC photolysis reaction contributed most substantially to RO_x production and the differences between the BASE and CON23 experiments. Fig. 4 compares OVOC photolysis in the two experiments averaged over the three photochemical cases (Supplementary Table S11). Formaldehyde was the most frequently photolyzed OVOC in both model experiments, consistent with previous findings in PRD [38]. In CON23, the second most commonly photolyzed OVOC was biacetyl (18%), but its photolysis was severely underestimated (4%) in the BASE experiments, which instead simulated substantial photolysis of methylglyoxal (26%); this value became minor (4%) when the

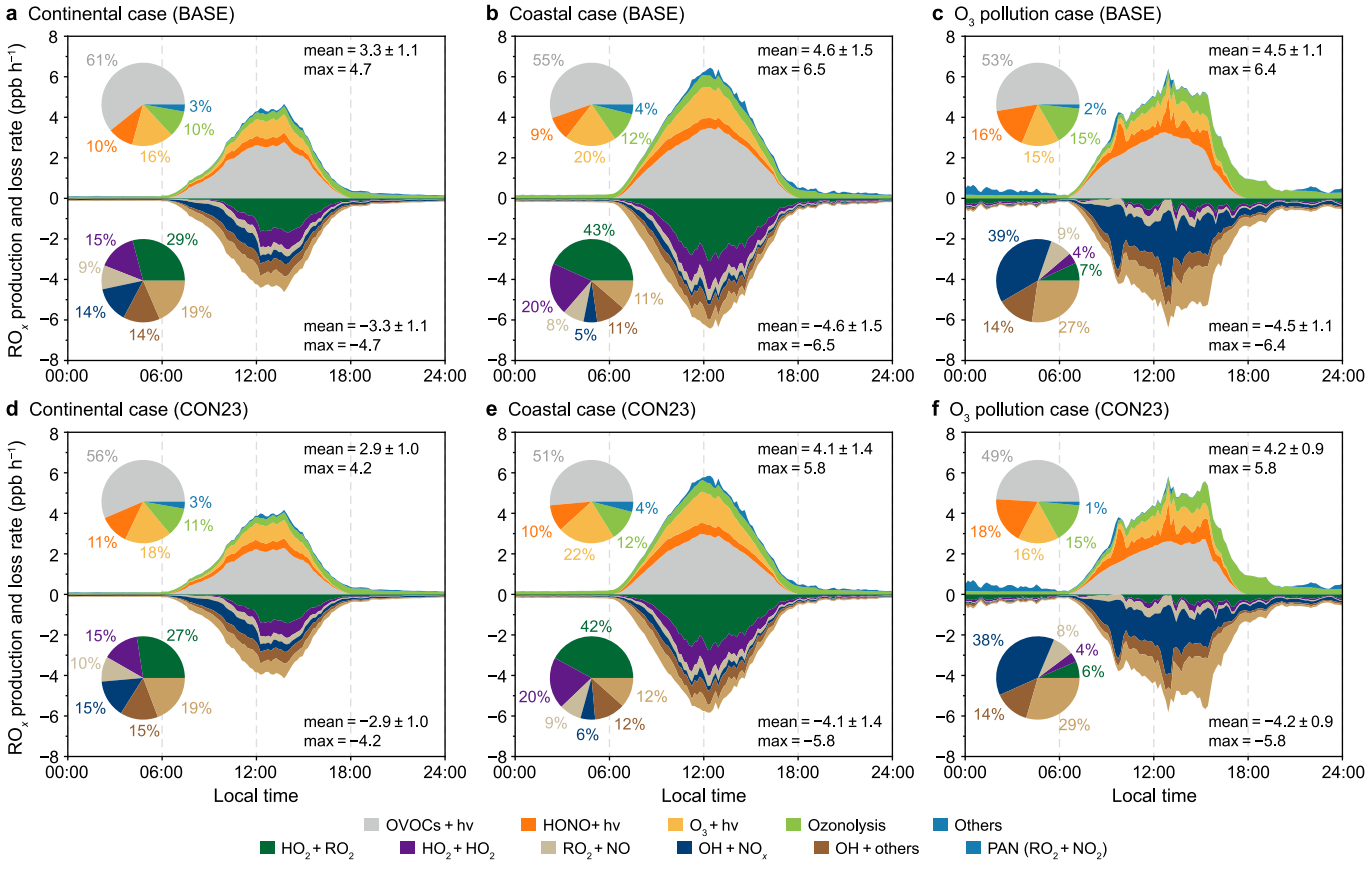

Fig. 3. Simulated diurnal variation of RO_x budgets and daytime pathway contributions. Stacked areas show RO_x budgets, and pie charts summarize the relative contributions of individual pathways during 06:00–18:00 local time. **a**–**c**, BASE experiments: continental (**a**), coastal (**b**), and O_3 pollution (**c**) cases. **d**–**f**, CON23 experiments: continental (**d**), coastal (**e**), and O_3 pollution (**f**) cases. $OH + NO_x$ indicated the sum of OH + NO and $OH + NO_2$. PAN indicated the net thermal decomposition of peroxyacetyl nitrate.

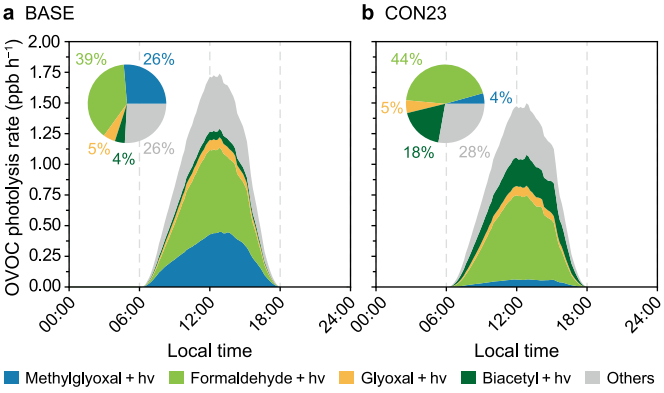

Fig. 4. Simulated diurnal variation in OVOC photolysis rates for the BASE (**a**) and CON23 (**b**) experiments. Values are averaged across the three photochemical cases.

methylglyoxal concentrations were constrained by measurements. The results from the three individual photochemical cases were also consistent (Supplementary Fig. S8).

We found that inaccuracies in the BASE experiments' OVOC photolysis values stemmed from biases in the simulated OVOC levels, which cascaded into errors across the RO_x budget. Comparisons with observations from across the sampling period (Fig. 5; Supplementary Table S6) revealed that the BASE experiments underestimated most OVOCs, especially biacetyl (−67%), while overestimating methylglyoxal (589%), MVK + MACR (275%), and benzaldehyde (55%). To contextualize the abundance and potential simulation biases of these OVOCs at HT, we first compared observed concentrations with previously reported values in China (Supplementary Tables S7 and S8). The observed average MVK + MACR concentration was 0.23 ppb, comparable to the value at another coastal background site in Shenzhen (0.26 ppb) [51] but half the figures reported from urban sites in the PRD (0.43–0.48 ppb) [19,52]. The consistently lower MVK + MACR levels at HT suggest distinct source–sink dynamics for these isoprene-derived OVOCs compared to urban environments. Methylglyoxal (0.15 ppb) and benzaldehyde (0.07 ppb) levels were consistently about 50% lower than urban concentrations [19,53,54]. In contrast, biacetyl (0.26 ppb) exhibited no consistent spatial pattern: the measured values were 17–32% higher than those in certain urban reports (0.31–0.38 ppb) [36,51] but 19–39% higher than other urban PRD measurements conducted in different years (0.16–0.21 ppb) [51], reflecting variability in emission sources or atmospheric processing.

Overall, these misrepresentations of key OVOC concentrations in the BASE experiments skewed the OH reactivity and the partitioning of OVOC photolysis, overattributing RO_x production to methylglyoxal and MVK + MACR while underrepresenting contributions from other OVOCs, particularly biacetyl (Supplementary Fig. S8). Critically, these OVOC errors propagated to the HO_2 and RO_2 production rates, which were 10–13% higher in BASE than in CON23 (Supplementary Fig. S6). Collectively, these findings underscore the necessity of precise OVOC quantification in models to avoid compounding errors in RO_x radical chemistry.

3.4. Potential causes of methylglyoxal and MVK + MACR overestimation in BASE experiments

Why did the BASE model perform relatively well in simulating OH concentrations but misrepresent OVOC levels and RO_x sources? Our analysis traced the BASE experiments' overestimation of methylglyoxal to inflated levels of MVK and MACR, two of methylglyoxal's key intermediate precursors from isoprene. Fig. S9 (Supplementary Material) shows that methylglyoxal was mostly produced from isoprene and aromatics, but its production from isoprene in the BASE experiments (0.22 ppb h^{-1}) was approximately twice as large as in the CON23 experiments (0.1 ppb h^{-1}). This overproduction was mainly due to higher contributions from the decomposition of the HMVKAO ($CH_3C(O)C(OH)CO\bullet$) radical and the ACETOL (hydroxyacetone) + OH reaction in the MCM (Supplementary Table S9). Both pathways stem from the photochemical oxidation of MVK and MACR [31,34].

The overestimation of methylglyoxal in the BASE experiment may also have arisen from a neglect of heterogeneous uptake on aqueous aerosols—a substantial sink for ambient methylglyoxal frequently excluded from box models such as the standard F0AM [34]. We added this sink to F0AM and evaluated its impact across a range of reactive uptake coefficients (γ_{MGLY}; Supplementary Text S2). Incorporating the heterogeneous uptake of methylglyoxal indeed reduced its simulated concentrations by 10%–56% (Fig. 5a). However, even with the largest γ_{MGLY}, the simulated methylglyoxal concentrations were still much higher than the observations. Therefore, the heterogeneous uptake of methylglyoxal could not fully resolve the discrepancy between simulations and observations, nor could it explain the overestimation of MVK and MACR. Nevertheless, our results highlight that aqueous uptake is an important sink for methylglyoxal and other OVOCs in humid environments, effectively suppressing OVOC gas-phase reactions while enhancing secondary organic aerosol formation [55,56].

It remains unclear why MVK and MACR were so severely

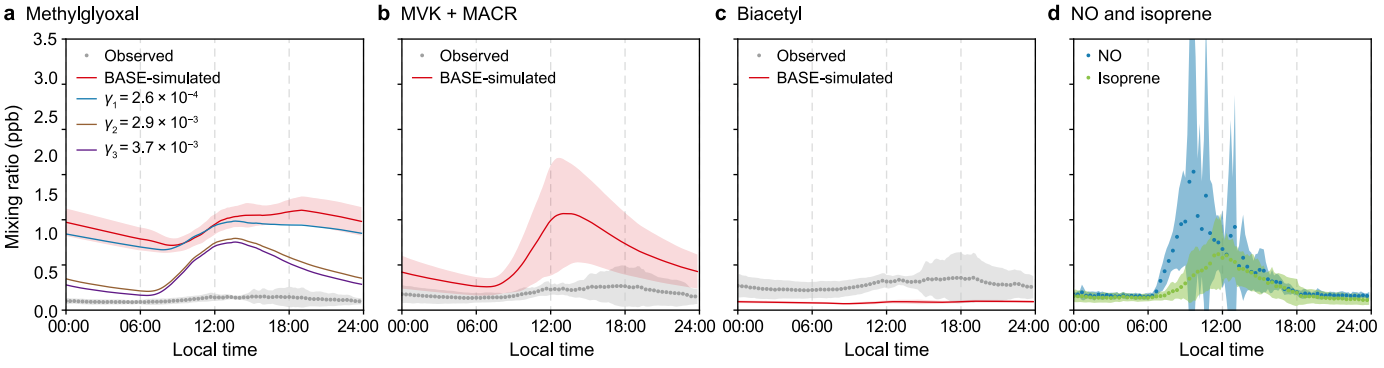

Fig. 5. **a**–**c**, Observed and BASE-simulated concentrations of methylglyoxal (**a**), MVK + MACR (**b**), and biacetyl (**c**). **d**, Observed concentrations of NO and isoprene. Values are averaged across the three photochemical cases; shading indicates the standard deviations. Panel **a** also shows methylglyoxal simulated with different heterogeneous uptake coefficients (γ) on wet aerosol surfaces (Supplementary Text S2).

overestimated in the BASE experiments despite the observational constraints on isoprene, given that the photochemical yields of MVK and MACR from isoprene have been well characterized across a wide range of NO_x levels [31]. We propose three mutually nonexclusive hypotheses. The first involves the origin and fate of isoprene sampled at HT. The elevated isoprene levels in the coastal case (Supplementary Table S3) may reflect marine emissions that are partially oxidized under lower NO_x conditions upwind. However, the box model interpreted this isoprene as reacting locally in HT's higher-NO_x environment, thereby accelerating MVK and MACR production. Second, MVK and MACR are both slightly water-soluble and thus susceptible to dry and wet depositions [57]—sinks often overlooked in box models and potentially underestimated by our assumed one-day physical lifetime. This underestimation of MVK and MACR removal might have led to these OVOCs overaccumulating in the simulations. Third, complexity arises from halogen chemistry. Cl (chlorine) radicals, an important booster of atmospheric oxidation capacity at HT [58], have recently been identified as a large sink for MVK [59,60]. We did not account for halogen chemistry in our F0AM experiments. Xia et al. [22] previously reported that direct RO_x production from bromine (Br_2) and Cl_2 was minor (approximately 4%) at HT, but the indirect effects of halogens on RO_x via MVK/MACR degradation pathways have not been explored.

3.5. Missing precursors or production pathways of biacetyl in MCM

The significant underestimation of biacetyl in the default model (−67%) and its insufficient representation in earlier studies highlight the need to better understand its sources and chemical reactions. The BASE model's underestimation of biacetyl contrasted sharply with the observed diurnal variations in biacetyl, indicating photochemical production (Fig. 5c). In the BASE simulation (based on the MCM), biacetyl was predominantly produced by trimethylbenzenes (54%) and xylenes (35%) (Supplementary Fig. S10 and Table S10). In the MCM, biacetyl was produced soon after ring cleavage of trimethylbenzenes and o-xylene, without forming many intermediate OVOC products. The concentrations of trimethylbenzenes and o-xylene were observationally constrained in both the BASE and CON23 experiments, such that the simulated biacetyl abundances and budgets were identical. Therefore, the above findings likely imply that (1) the yields of biacetyl from trimethylbenzenes and o-xylene were much too low in the MCM, and (2) important primary precursors or production pathways of biacetyl were missing in the MCM.

3.6. Sensitivity tests for quantifying the contributions of key OVOCs

Our analysis in Section 3.3 showed that the biases in BASE-simulated methylglyoxal and biacetyl offset simulated OVOC photolysis (Fig. 4, Supplementary Table S11) and RO_x production, which may complexly impact downstream O_3 production. We conducted further sensitivity experiments to isolate their individual impacts relative to the BASE experiments, averaged over all photochemical cases (Supplementary Text S3 and Fig. S11). We found that adding methylglyoxal constraints to BASE decreased OVOC photolysis by up to 29%, substantially reducing RO_x production (−15%) and abundance (−10%) as well as O_3 production (−13%). In contrast, adding only MVK and MACR constraints to BASE would increase OH levels (8.9%) by reducing these species' OH consumption (Supplementary Fig. S11), while OVOC photolysis (−18%), RO_x production (−10%), and HO_2 (−6.3%) and RO_2 (−16%) abundance were still reduced. MVK and MACR acted mainly as sinks to OH during the campaign, while their photochemical product, methylglyoxal, contributed substantially to RO_x production.

The addition of biacetyl constraints to BASE would increase RO_x abundance and accelerate RO_x cycling, eventually accelerating O_3 production by 6.7%. Finally, if methylglyoxal, MVK, MACR, and biacetyl measurements were simultaneously applied to constrain the box model, the net OH decrease over the BASE experiments would be slight (−0.3%, Supplementary Fig. S11). Comparing this result to that of the CON23 experiment, we concluded the following: While the photochemical impacts of other minor OVOCs were individually small, their combined impacts on OH, RO_x cycling, and O_3 production remained substantial, highlighting the necessity of observationally constraining a broad suite of OVOCs in photochemical budget studies.

3.7. Impacts of OVOC observational constraints on simulated O_x production and sensitivity regimes

Finally, we explored how improving the simulated RO_x budgets by constraining OVOC abundance affected the simulated O_3 production at HT in the fall. Fig. 6 compares the simulated O_3 budgets for the three photochemical cases. The local O_3 production rate ($P(O_3)$, Supplementary Text S2) was highest in the O_3 pollution case, followed by the coastal case and the continental case. In all cases, and regardless of OVOC constraints, the RO_2 + NO (55%) reaction was the largest contributor to O_3 production, exceeding HO_2 + NO (45%). This finding contrasted with an earlier study at HT under high-NO_x conditions [20] and with findings from a remote island site in the South China Sea [61]. The dominance of the RO_2 + NO pathway was similar to that previously characterized at a rural site in Central China, another low-NO_x location affected by aged, polluted air [62]. The simulated loss of O_3 ($L(O_3)$, Supplementary Text S2e) was dominated by O_3 photolysis (36–52%, 0.52–0.89 ppb h^{-1}) in the non-ozone pollution cases, while OH + NO_2 (48–50%, 1.4–1.6 ppb h^{-1}) yielded the largest loss of O_3 in the pollution case.

Constraining the abundances of more OVOC species reduced the simulated maximum $P(O_3)$ as much as 17% (Fig. 6) by decreasing the simulated OH oxidant levels (Fig. 2) and altering the simulated RO_2 levels and compositions (Supplementary Fig. S6 and Table S4). We identified the ten RO_2 + NO pathways that contributed most to O_3 production (Supplementary Table S12), accounting for 54–58% of the total RO_2 + NO reaction rates and 29–33% of the total $P(O_3)$. The two RO_2 species responsible for the largest $P(O_3)$ values were CH_3O_2 (methylperoxy radical, 24%) and CH_3CO_3 (acetylperoxy radical, 17%), which are produced downstream of the photochemical oxidation of all VOCs from anthropogenic and biogenic sources [63], including methylglyoxal and biacetyl. Peroxy radicals from isoprene ($ISOPBO_2$, $ISOPDO_2$, and $HMVKBO_2$) and butenes (BUT_2OLO_2 and $NBUTOLAO_2$) also contributed significantly to local O_3 production via RO_2 + NO reactions. Constraining the box model with the observed abundances of 23 OVOC species decreased the simulated abundance of $HMVKBO_2$ (produced downstream of MVK from isoprene), decreased those of CH_3O_2 and CH_3CO_3 (downstream of many OVOCs, including methylglyoxal and biacetyl), and increased those of other minor RO_2 species.

The sensitivity of local O3 production to different OVOC observational constraints is shown in Fig. S12 (Supplementary Material). Local O_3 production at HT in fall 2020 was generally NO_x-sensitive, except during the O_3 pollution event. Constraining the photochemical model with the observations of more OVOC species significantly increased the relative incremental reactivity (RIR) values of OVOCs by a factor of 2–5 but decreased the sensitivity of local O_3 production to other primary VOC precursors from anthropogenic and biogenic sources. This feature highlights the role of reactive OVOC intermediates in local ozone formation at HT.

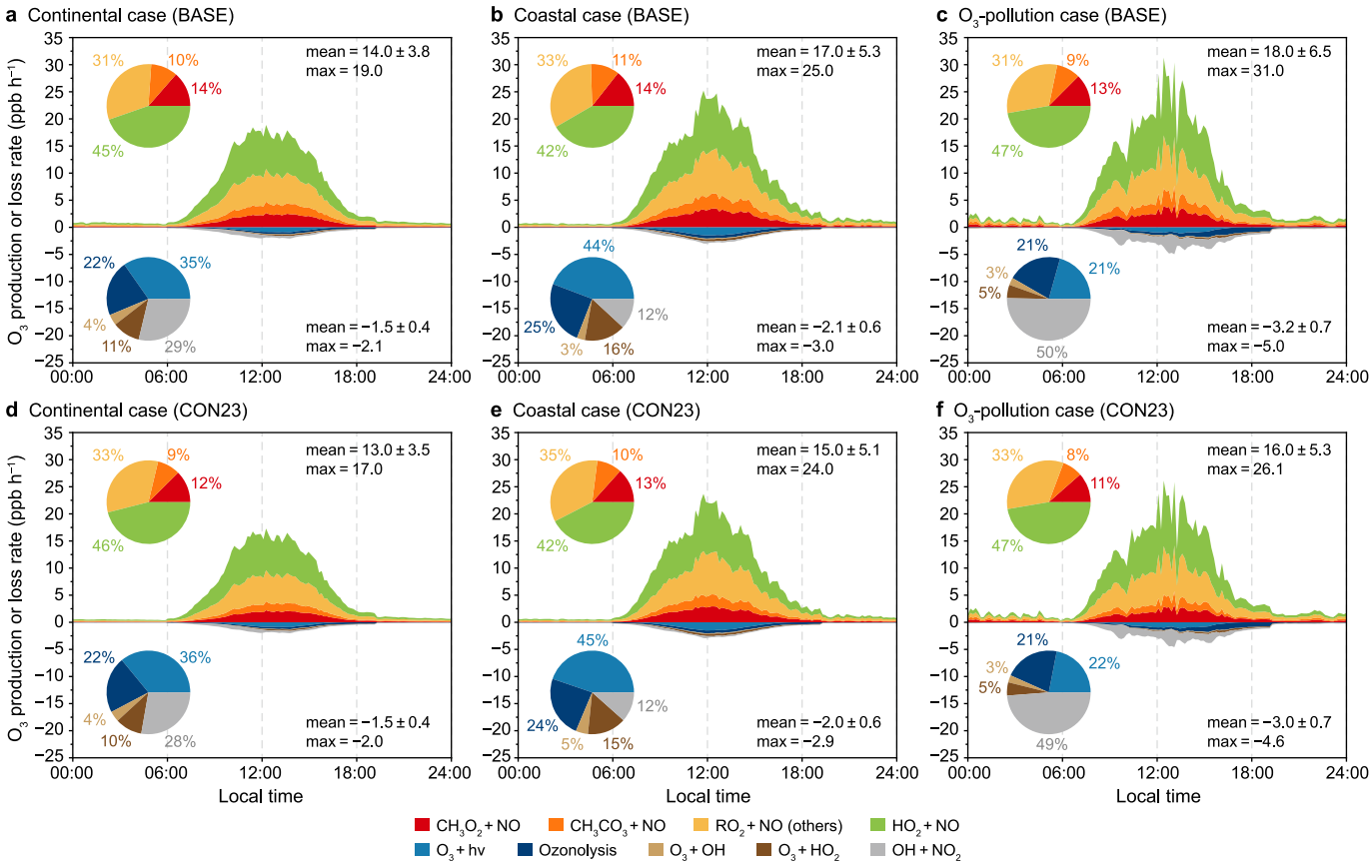

Fig. 6. Simulated diurnal variation of O_3 budgets and daytime mean process contributions. Stacked areas show the simulated diurnal O_3 budgets, and pie charts summarize mean contributions of individual production (top) and loss (bottom) processes during 09:00–17:00 local time. **a**–**c**, BASE experiments: continental (**a**), coastal (**b**), and O_3 pollution (**c**) cases. **d**–**f**, CON23 experiments: continental (**d**), coastal (**e**), and O_3 pollution (**f**) cases.

Furthermore, the simulated O_3 sensitivity exhibited a substantial reduction in NO_x saturation during the O_3 pollution event. Therefore, imposing additional observational constraints on OVOC abundance provided better guidance for emission control strategies to mitigate local O_3 production.

4. Conclusions

In this study, we demonstrate the need to observationally constrain more OVOC species, beyond the typical three OVOCs (formaldehyde, acetaldehyde, and acetone) and particularly dicarbonyls, to accurately represent local photochemistry. At HT, the inclusion of 23 OVOCs in the simulations improved simulated OH levels to the point that they were consistent with observations within the measurement uncertainty. In addition, *in situ* RO_x and O_3 budget analyses indicated changes in the chemical conditions of the regional background atmosphere at HT compared with 2012. Photolysis of OVOC was the largest RO_x source, while $RO_2 + NO$ was the largest local O_3 production pathway. This underlines the growing role of OVOCs in driving O_3 production in the PRD.

Our findings highlight several critical priorities for future observational and modeling studies. Future field campaigns should expand *in situ* measurements of dicarbonyls and other reactive OVOCs, both at the surface and in the boundary layer. Recent studies have indicated significant accumulation and vigorous photochemistry of OVOCs in the boundary layer, which influence the surface through vertical mixing [42,64]. However, our model assumed a well-mixed box and could not capture this layered photochemical processing. Emerging tools, such as remote sensing of methylglyoxal and biacetyl, next-generation sensors, and deep learning frameworks, show promise in achieving high-resolution, vertically resolved, and more accurate OVOC measurements [11,12]. Concurrently, model representations of OVOC chemistry must be refined, particularly with respect to multiphase and photochemical mechanisms. Integrating box modeling with regional-scale simulations would provide a more holistic understanding of OVOC budgets, and rigorous evaluation against both *in situ* and remote sensing data will be essential to identify and address key knowledge gaps.

CRediT authorship contribution statement

Enyu Xiong: Writing - Original Draft, Visualization, Validation, Software, Methodology, Investigation, Data Curation, Conceptualization. **Hai Guo:** Writing - Review & Editing, Supervision, Resources, Project administration, Funding Acquisition, Data Curation, Conceptualization. **Tzung-May Fu:** Writing - Review & Editing, Supervision, Resources, Project Administration, Funding Acquisition, Data Curation, Conceptualization. **Xiaopu Lyu:** Validation, Methodology, Formal Analysis. **Yu Wang:** Validation, Investigation. **Beining Zhou:** Validation, Software, Investigation. **Men Xia:** Validation, Investigation, Data Curation. **Zhouxing Zou:** Validation, Investigation, Data Curation. **Qi Yuan:** Validation, Investigation, Data Curation. **Jin Yang:** Validation, Investigation, Data Curation. **Kit Ying Shek:** Data Curation, Investigation, Validation. **Jiongkai Chen:** Visualization, Software. **Tianci Jiang:**

Visualization, Software. **Wei Tao:** Validation, Formal Analysis. **Aoxing Zhang:** Validation, Software, Formal Analysis. **Wang Xiang:** Software, Formal Analysis. **Shuncheng Lee:** Investigation, Data Curation. **Tao Wang:** Resources, Project Administration, Investigation, Funding Acquisition.

Data availability statement

The VOCs data used in this study are available upon request from the authors.

Declaration of competing interest

The authors declare that they have no known competing financial interests or personal relationships that could have appeared to influence the work reported in this paper.

Acknowledgements

This research was funded by the Hong Kong Research Grants Council via Theme-Based Research Scheme (T24-504/17-N) and General Research Fund (HKBU 15219621), the National Natural Science Foundation of China (42325504), the National Key Research and Development Program of China (2023YFC3706205), and the Shenzhen Science and Technology Program (JCYJ20220818100611024). Computational resources were supported by the Center for Computational Science and Engineering at the Southern University of Science and Technology. The authors would like to thank the Hong Kong Environmental Protection Department for providing the field study site and the Hong Kong Observatory for providing the meteorological data. The authors are grateful to Jazz Chan and Steven Poon for their technical support during the field campaign.

Appendix A. Supplementary data

Supplementary data to this article can be found online at https://doi.org/10.1016/j.ese.2026.100659.

References

[1] Ministry of Ecology and Environment PRC, Report on the state of the ecology and environment in China. https://english.mee.gov.cn/Resources/Reports/soe/, 2023. (Accessed 26 March 2024), 2024.
[2] T. Cao, H. Wang, L. Li, X. Lu, Y. Liu, et al., Fast spreading of surface ozone in both temporal and spatial scale in Pearl River Delta, J. Environ. Sci. 137 (2024) 540–552, https://doi.org/10.1016/j.jes.2023.02.025.
[3] Department of ecology and environment of Guangdong province, report on the state of Guangdong provincial ecology and environment 2023. https://gdee.gd.gov.cn/gkmlpt/content/4/4746/post_4746330.html#3185, 2024. (Accessed 4 May 2024).
[4] K. Lu, S. Guo, Z. Tan, H. Wang, D. Shang, et al., Exploring atmospheric free-radical chemistry in China: the self-cleansing capacity and the formation of secondary air pollution, Natl. Sci. Rev. 6 (2019) 579–594, https://doi.org/10.1093/nsr/nwy073.
[5] J.H. Seinfeld, S.H. Pandis, Atmospheric Chemistry and Physics: from Air Pollution to Climate Change, third ed., John Wiley & Sons, Inc., Hoboken, New Jersey, 2016.
[6] D.J. Lary, D.E. Shallcross, Central role of carbonyl compounds in atmospheric chemistry, J. Geophys. Res. Atmos. 105 (2000) 19771–19778, https://doi.org/10.1029/1999jd901184.
[7] Q. Liu, Y. Gao, W. Huang, Z. Ling, Z. Wang, et al., Carbonyl compounds in the atmosphere: a review of abundance, source and their contributions to O_3 and SOA formation, Atmos. Res. 274 (2022) 106184, https://doi.org/10.1016/j.atmosres.2022.106184.
[8] Y. Cheng, X.F. Huang, Y. Peng, L.M. Cao, X. Peng, et al., Enhancing time resolution of ambient VOC measurement data by machine learning: from one-hour to five minutes, J. Geophys. Res. Atmos. 130 (2025), https://doi.org/10.1029/2024JD042477 e2024JD042477.
[9] C. Wu, C. Wang, S. Wang, W. Wang, B. Yuan, et al., Measurement report: important contributions of oxygenated compounds to emissions and chemistry of volatile organic compounds in urban air, Atmos. Chem. Phys. 20 (2020) 14769–14785, https://doi.org/10.5194/acp-20-14769-2020.
[10] S. Wang, B. Yuan, C. Wu, C. Wang, T. Li, et al., Oxygenated volatile organic compounds (VOCs) as significant but varied contributors to VOC emissions from vehicles, Atmos. Chem. Phys. 22 (2022) 9703–9720, https://doi.org/10.5194/acp-22-9703-2022.
[11] S. Zhu, J. Xu, M. Fan, C. Yu, H. Letu, et al., Estimating near-surface concentrations of major air pollutants from space: a universal estimation framework LAPSO, IEEE Trans. Geosci. Rem. Sens. 61 (2023) 1–11, https://doi.org/10.1109/tgrs.2023.3248180.
[12] J. Xu, Z. Zhang, L. Rao, Y. Wang, H. Letu, et al., Remote sensing of tropospheric ozone from space: progress and challenges, J. Remote Sens. 4 (2024) 178, https://doi.org/10.34133/remotesensing.0178.
[13] Z. Zou, Q. Chen, M. Xia, Q. Yuan, Y. Chen, et al., OH measurements in the coastal atmosphere of South China: possible missing OH sinks in aged air masses, Atmos. Chem. Phys. 23 (2023) 7057–7074, https://doi.org/10.5194/acp-23-7057-2023.
[14] X. Yang, H. Wang, K. Lu, X. Ma, Z. Tan, et al., Reactive aldehyde chemistry explains the missing source of hydroxyl radicals, Nat. Commun. 15 (2024) 1648, https://doi.org/10.1038/s41467-024-45885-w.
[15] A. Hofzumahaus, F. Rohrer, K. Lu, B. Bohn, T. Brauers, C.-C.C.C. Chang, H. Fuchs, F. Holland, K. Kita, Y. Kondo, X. Li, S. Lou, M. Shao, L. Zeng, A. Wahner, Y. Zhang, Amplified trace gas removal in the troposphere, Science 324 (2009) 1702–1704, https://doi.org/10.1126/science.1164566.
[16] X. Yang, Y. Li, X. Ma, Z. Tan, K. Lu, et al., Unclassical radical generation mechanisms in the troposphere: a review, Environ. Sci. Technol. 58 (2024) 36, https://doi.org/10.1021/acs.est.4c00742.
[17] K. Li, D.J. Jacob, H. Liao, Y. Qiu, L. Shen, et al., Ozone pollution in the North China Plain spreading into the late-winter haze season, Proc. Natl. Acad. Sci. 118 (2021) e2015797118, https://doi.org/10.1073/pnas.2015797118.
[18] H. Qu, Y. Wang, R. Zhang, X. Liu, L.G. Huey, et al., Chemical production of oxygenated volatile organic compounds strongly enhances boundary-layer oxidation chemistry and ozone production, Environ. Sci. Technol. 55 (2021) 13718–13727, https://doi.org/10.1021/acs.est.1c04489.
[19] W. Wang, B. Yuan, Y. Peng, H. Su, Y. Cheng, et al., Direct observations indicate photodegradable oxygenated volatile organic compounds (OVOCs) as larger contributors to radicals and ozone production in the atmosphere, Atmos. Chem. Phys. 22 (2022) 4117–4128, https://doi.org/10.5194/acp-22-4117-2022.
[20] Z. Li, L. Xue, X. Yang, Q. Zha, Y.J. Tham, et al., Oxidizing capacity of the rural atmosphere in Hong Kong, Southern China, Sci. Total Environ. 612 (2018) 1114–1122, https://doi.org/10.1016/j.scitotenv.2017.08.310.
[21] H. Wang, X. Lyu, H. Guo, Y. Wang, S. Zou, et al., Ozone pollution around a coastal region of South China Sea: interaction between marine and continental air, Atmos. Chem. Phys. 18 (2018) 4277–4295, https://doi.org/10.5194/acp-18-4277-2018.
[22] Z. Tan, F. Rohrer, K. Lu, X. Ma, B. Bohn, et al., Wintertime photochemistry in Beijing: observations of RO_x radical concentrations in the North China Plain during the BEST-ONE campaign, Atmos. Chem. Phys. 18 (2018) 12391–12411, https://doi.org/10.5194/acp-18-12391-2018.
[23] X. Ma, Z. Tan, K. Lu, X. Yang, Y. Liu, et al., Winter photochemistry in Beijing: observation and model simulation of OH and HO_2 radicals at an urban site, Sci. Total Environ. 685 (2019) 85–95, https://doi.org/10.1016/j.scitotenv.2019.05.329.
[24] X. Yang, K. Lu, X. Ma, Y. Gao, Z. Tan, et al., Radical chemistry in the Pearl River Delta: observations and modeling of OH and HO_2 radicals in Shenzhen in 2018, Atmos. Chem. Phys. 22 (2022) 12525–12542, https://doi.org/10.5194/acp-22-12525-2022.
[25] Y. Xu, X. Feng, Y. Chen, P. Zheng, L. Hui, et al., Development of an enhanced method for atmospheric carbonyls and characterizing their roles in photochemistry in subtropical Hong Kong, Sci. Total Environ. 896 (2023) 165135, https://doi.org/10.1016/j.scitotenv.2023.165135.
[26] M. Xia, T. Wang, Z. Wang, Y. Chen, X. Peng, et al., Pollution-derived Br_2 boosts oxidation power of the coastal atmosphere, Environ. Sci. Technol. 56 (2022) 12055–12065, https://doi.org/10.1021/acs.est.2c02434.
[27] Q. Yuan, Z. Zhang, Y. Chen, L. Hui, M. Wang, et al., Origin and transformation of volatile organic compounds at a regional background site in Hong Kong: varied photochemical processes from different source regions, Sci. Total Environ. 908 (2024) 168316, https://doi.org/10.1016/j.scitotenv.2023.168316.
[28] A.F. Stein, M.D. Cohen, B.J.B. Stunder, G.D. Rolph, R.R. Draxler, et al., NOAA's HYSPLIT atmospheric transport and dispersion modeling system, B. Am. Meteorol. Soc. 96 (2015) 2059–2077, https://doi.org/10.1175/bams-d-14-00110.1.
[29] N. Wang, X. Huang, J. Xu, T. Wang, Z.-M. Tan, et al., Typhoon-boosted biogenic emission aggravates cross-regional ozone pollution in China, Sci. Adv. 8 (2022), https://doi.org/10.1126/sciadv.abl6166 eab16166.
[30] G.M. Wolfe, M.R. Marvin, S.J. Roberts, K.R. Travis, J. Liao, The framework for 0-D atmospheric modeling (F0AM) v3.1, Geosci. Model Dev. (GMD) 9 (2016) 3309–3319, https://doi.org/10.5194/gmd-9-3309-2016.
[31] M.E. Jenkin, J.C. Young, A.R. Rickard, The MCM v3.3.1 degradation scheme for isoprene, Atmos. Chem. Phys. 15 (2015) 11433–11459, https://doi.org/10.5194/acp-15-11433-2015.
[32] S.M. Saunders, M.E. Jenkin, R.G. Derwent, M.J. Pilling, Protocol for the development of the master chemical mechanism v3 (Part A): tropospheric degradation of non-aromatic volatile organic compounds, Atmos. Chem.

Phys. 3 (2003) 161–180, https://doi.org/10.5194/acp-3-161-2003.
[33] M.E. Jenkin, S.M. Saunders, V. Wagner, M.J. Pilling, Protocol for the development of the master chemical mechanism, MCM v3 (Part B): tropospheric degradation of aromatic volatile organic compounds, Atmos. Chem. Phys. 3 (2003) 181–193, https://doi.org/10.5194/acp-3-181-2003.
[34] T.-M. Fu, D.J. Jacob, F. Wittrock, J.P. Burrows, M. Vrekoussis, et al., Global budgets of atmospheric glyoxal and methylglyoxal, and implications for formation of secondary organic aerosols, J. Geophys. Res. 113 (2008) D15, https://doi.org/10.1029/2007jd009505.
[35] Z. Ling, Q. Xie, M. Shao, Z. Wang, T. Wang, et al., Formation and sink of glyoxal and methylglyoxal in a polluted subtropical environment: observation-based photochemical analysis and impact evaluation, Atmos. Chem. Phys. 20 (2020) 11451–11467, https://doi.org/10.5194/acp-20-11451-2020.
[36] L. Hui, X. Feng, Q. Yuan, Y. Chen, Y. Xu, et al., Abundant oxygenated volatile organic compounds and their contribution to photochemical pollution in subtropical Hong Kong, Environ. Pollut. 335 (2023) 122287, https://doi.org/10.1016/j.envpol.2023.122287.
[37] Y. Tan, S. Han, Y. Chen, Z. Zhang, H. Li, et al., Characteristics and source apportionment of volatile organic compounds (VOCs) at a coastal site in Hong Kong, Sci. Total Environ. 777 (2021) 146241, https://doi.org/10.1016/j.scitotenv.2021.146241.
[38] H. Shen, Y. Liu, M. Zhao, J. Li, Y. Zhang, et al., Significance of carbonyl compounds to photochemical ozone formation in a coastal city (Shantou) in eastern China, Sci. Total Environ. 764 (2021) 144031, https://doi.org/10.1016/j.scitotenv.2020.144031.
[39] S. Yang, B. Yuan, Y. Peng, S. Huang, W. Chen, et al., The formation and mitigation of nitrate pollution: comparison between urban and suburban environments, Atmos. Chem. Phys. 22 (2022) 4539–4556, https://doi.org/10.5194/acp-22-4539-2022.
[40] D. Yu, Z. Tan, K. Lu, X. Ma, X. Li, et al., An explicit study of local ozone budget and NO_x-VOCs sensitivity in Shenzhen China, Atmos. Environ. 224 (2020) 117304, https://doi.org/10.1016/j.atmosenv.2020.117304.
[41] Y. Meng, J. Song, L. Zeng, Y. Zhang, Y. Zhao, et al., Ambient volatile organic compounds at a receptor site in the Pearl River Delta region: variations, source apportionment and effects on ozone formation, J. Environ. Sci. 111 (2022) 104–117, https://doi.org/10.1016/j.jes.2021.02.024.
[42] X.-B. Li, B. Yuan, S. Wang, C. Wang, J. Lan, et al., Variations and sources of volatile organic compounds (VOCs) in urban region: insights from measurements on a tall tower, Atmos. Chem. Phys. 22 (2022) 10567–10587, https://doi.org/10.5194/acp-22-10567-2022.
[43] Y. Liu, J. Li, Y. Ma, M. Zhou, Z. Tan, et al., A review of gas-phase chemical mechanisms commonly used in atmospheric chemistry modelling, J. Environ. Sci. 123 (2023) 522–534, https://doi.org/10.1016/j.jes.2022.10.031.
[44] S.M. Griffith, R.F. Hansen, S. Dusanter, V. Michoud, J.B. Gilman, et al., Measurements of hydroxyl and hydroperoxy radicals during CalNex-LA: model comparisons and radical budgets, J. Geophys. Res. Atmos. 121 (2016) 4211–4232, https://doi.org/10.1002/2015jd024358.
[45] L.K. Whalley, D. Stone, R. Dunmore, J. Hamilton, J.R. Hopkins, et al., Understanding in situ ozone production in the summertime through radical observations and modelling studies during the clean air for London project (ClearfLo), Atmos. Chem. Phys. 18 (2018) 2547–2571, https://doi.org/10.5194/acp-18-2547-2018.
[46] Z. Tan, K. Lu, A. Hofzumahaus, H. Fuchs, B. Bohn, et al., Experimental budgets of OH, HO2 and RO2 radicals and implications for ozone formation in the Pearl River Delta in China 2014, Atmos. Chem. Phys. 19 (2019) 7129–7150, https://doi.org/10.5194/acp-19-7129-2019.
[47] C. Xue, C. Ye, J. Kleffmann, W. Zhang, X. He, et al., Atmospheric measurements at mt. Tai – part II: HONO budget and radical ($RO_x + NO_3$) chemistry in the lower boundary layer, Atmos. Chem. Phys. 22 (2022) 1035–1057, https://doi.org/10.5194/acp-22-1035-2022.
[48] Z. Tan, K. Lu, M. Jiang, R. Su, H. Wang, et al., Daytime atmospheric oxidation capacity in four Chinese megacities during the photochemically polluted season: a case study based on box model simulation, Atmos. Chem. Phys. 19 (2019) 3493–3513, https://doi.org/10.5194/acp-19-3493-2019.
[49] B. Bottorff, M.M. Lew, Y. Woo, P. Rickly, M.D. Rollings, et al., OH, HO_2, and RO_2 radical chemistry in a rural forest environment: measurements, model comparisons, and evidence of a missing radical sink, Atmos. Chem. Phys. 23 (2023) 10287–10311, https://doi.org/10.5194/acp-23-10287-2023.
[50] X. Lyu, H. Li, S.-C. Lee, E. Xiong, H. Guo, et al., Significant biogenic source of oxygenated volatile organic compounds and the impacts on photochemistry at a regional background site in South China, Environ. Sci. Technol. 58 (2024) 20081–20090, https://doi.org/10.1021/acs.est.4c05656.
[51] S.-Y. Xia, B. Zhu, S.-X. Wang, X.-F. Huang, L.-Y. He, Spatial distribution and source apportionment of peroxyacetyl nitrate (PAN) in a coastal region in southern China, Atmos. Environ. 260 (2021) 118553, https://doi.org/10.1016/j.atmosenv.2021.118553.
[52] J. Guo, G. Zhang, R. Hu, P. Xie, C. Hu, et al., Local radical chemistry driven ozone pollution in a megacity: a case study, Atmos. Environ. 318 (2024) 120227, https://doi.org/10.1016/j.atmosenv.2023.120227.
[53] Z. Wu, Y. Zhang, C. Pei, Z. Huang, Y. Wang, et al., Real-world emissions of carbonyls from vehicles in an urban tunnel in south China, Atmos. Environ. 258 (2021) 118491, https://doi.org/10.1016/j.atmosenv.2021.118491.
[54] M. Yang, F. Li, C. Huang, L. Tong, X. Dai, et al., VOC characteristics and their source apportionment in a coastal industrial area in the Yangtze River Delta, China, J. Environ. Sci. 127 (2023) 483–494, https://doi.org/10.1016/j.jes.2022.05.041.
[55] Y. Liu, B. Shi, W. Wang, Y. Guo, Y. Zeng, et al., Effects of aqueous environments and the water molecule on the degradation mechanism of methylglyoxal initiated by OH radicals: a theoretical study, ACS Earth Space Chem. 9 (2025) 934–943, https://doi.org/10.1021/acsearthspacechem.5c00013.
[56] Y. Zhang, R. Zhang, C.K. Chan, M. He, B. Wei, et al., Theoretical investigation on the oxidation mechanism of methylglyoxal in the aqueous phase, Chemosphere 366 (2024) 143425, https://doi.org/10.1016/j.chemosphere.2024.143425.
[57] B. Ervens, P. Renard, S. Tlili, S. Ravier, J.L. Clément, et al., Aqueous-phase oligomerization of methyl vinyl ketone through photooxidation – part 2: development of the chemical mechanism and atmospheric implications, Atmos. Chem. Phys. 15 (2015) 9109–9127, https://doi.org/10.5194/acp-15-9109-2015.
[58] X. Peng, T. Wang, W. Wang, A.R. Ravishankara, C. George, et al., Photodissociation of particulate nitrate as a source of daytime tropospheric Cl_2, Nat. Commun. 13 (2022) 939, https://doi.org/10.1038/s41467-022-28383-9.
[59] Z. Ding, S. Tian, J. Dang, Q. Zhang, New mechanistic understanding for atmospheric oxidation of isoprene initiated by atomic chlorine, Sci. Total Environ. 801 (2021), https://doi.org/10.1016/j.scitotenv.2021.149768.
[60] X. Wang, L. Bao, D. Han, Y. Wei, M. He, et al., Theoretical investigation on the degradation of methyl vinyl ketone initiated by ·OH and ·cl in the atmosphere and aqueous particles: mechanism, kinetics, and environmental impact analysis, Atmos. Environ. 246 (2021) 118107, https://doi.org/10.1016/j.atmosenv.2020.118107.
[61] Y. Wang, H. Guo, S. Zou, X. Lyu, Z. Ling, et al., Surface O_3 photochemistry over the South China Sea: application of a near-explicit chemical mechanism box model, Environ. Pollut. 234 (2018) 155–166, https://doi.org/10.1016/j.envpol.2017.11.001.
[62] X. Lyu, H. Guo, W. Zhang, H. Cheng, D. Yao, et al., Ozone and its precursors in a high-elevation and highly forested region in central China: origins, in-situ photochemistry and implications of regional transport, Atmos. Environ. 259 (2021) 118540, https://doi.org/10.1016/j.atmosenv.2021.118540.
[63] X. Liu, N. Wang, X. Lyu, Y. Zeren, F. Jiang, et al., Photochemistry of ozone pollution in autumn in Pearl River Estuary, South China, Sci. Total Environ. 754 (2021) 141812, https://doi.org/10.1016/j.scitotenv.2020.141812.
[64] F. Kluge, T. Hüneke, M. Knecht, M. Lichtenstern, M. Rotermund, et al., Profiling of formaldehyde, glyoxal, methylglyoxal, and CO over the amazon: normalized excess mixing ratios and related emission factors in biomass burning plumes, Atmos. Chem. Phys. 20 (2020) 12363–12389, https://doi.org/10.5194/acp-20-12363-2020.